LAWRENCE
LIVERMORE
NATIONAL
LABORATORY

LLNL-JRNL-644033

Highly Mobile AlHx Species and the Dehydrogenation Kinetics of NaAlH4

F. Zhang, B. Wood, Y. Wang, C. Z. Wang, K. M. Ho, M. Y. Chou

September 19, 2013

Journal of Physical Chemistry C

Disclaimer

Highly mobile AlH_x species and the dehydrogenation kinetics of $NaAlH_4$

Feng Zhang,[1,2] Brandon Wood,[3] Yan Wang,[1] C. Z. Wang,[2] K. M. Ho,[2] and M. Y. Chou[1,4,*]

[1]*School of Physics, Georgia Institute of Technology, Atlanta, GA 30332, USA*

[2]*Ames Laboratory, US Department of Energy, Ames, Iowa 50011, USA*

[3]*Lawrence Livermore National Laboratory, Livermore, CA 94551, USA*

[4]*Institute of Atomic and Molecular Sciences, Academia Sinica, Taipei 10617, Taiwan*

(Dated: September 3, 2013)

Abstract

The diffusion of Al-bearing species via AlH_x vacancies in γ-$NaAlH_4$ is investigated with first-principles calculations. For both charged AlH_4^- and neutral AlH_3 vacancies, the energy barriers for the diffusion are less than 0.1 eV, low enough that the predicted diffusion pathways are directly observable in first-principles molecular dynamics (FPMD) simulations on picosecond time-scales. In contrast, such diffusion in the α phase is inaccessible to FPMD simulations, consistent with its much larger energy barriers. These findings strongly support that a transition from the α phase to the γ phase or one of its high-entropy relatives facilitates the hydrogen-releasing decomposition of $NaAlH_4$. They also provide an answer to long-standing questions regarding the responsible agent for the experimentally observed efficient mass transport during dehydrogenation.

The identification of a suitable hydrogen storage system to pair with a hydrogen fuel cell remains a major challenge for developing a hydrogen economy [1]. Sodium alanate ($NaAlH_4$), a prototypical complex metal hydride that can release 5.3 wt% hydrogen, has been the focus of attention as a promising candidate since it was found that a small amount of early transition metals such as Ti can dramatically improve its reaction kinetics [2]. Even today, lightly doped $NaAlH_4$ remains a front runner among all candidates under comprehensive criteria that include hydrogen capacity, operating temperature, and price [3].

Despite extensive studies for over a decade, the exact pathways for the hydrogen-releasing decomposition of $NaAlH_4$ remain largely enigmatic. *In situ* X-ray diffraction studies showed multiple unidentified intermediate phases [4]. The narrow width of the diffraction peaks, corresponding to relatively large grain sizes (>100 nm) of Al crystallites [4], indicated that there must be an efficient channel for long-range transport of Al-bearing species. Since then, several other experimental studies have pointed to the presence of highly mobile AlH_x species, with reported barriers as low as 0.126 eV [5–9]. However, the extremely fast diffusion of such species in the conventional α phase of $NaAlH_4$ is not supported by theoretical calculations, which demonstrate that the diffusion of AlH_x needs to overcome much larger energy barriers [10, 11]. The above information combined strongly suggests that a new intermediate phase with easier Al diffusion participates in the decomposition of $NaAlH_4$.

Recently, theoretical calculations have shown that other polymorphs of $NaAlH_4$ could be thermodynamically more stable than the α phase at temperatures relevant for dehydrogenation, particularly near exposed surfaces. The nucleation of these phases at surfaces could be related to the enhanced kinetics observed for nano-confined $NaAlH_4$ [12–14] and for ball-milled samples [15]. Such polymorphs include a γ phase with the space group $Cmcm$ [16], and another structure with $Fmm2$ symmetry that significantly resembles the γ phase [17]. The γ phase successfully reproduces an experimentally observed [18] Raman peak at 1800 cm^{-1}, and both phases demonstrate X-ray diffraction features in common with unknowns observed by Gross *et al.* [4]. In addition, both the $Cmcm$ and $Fmm2$ phases feature large free volume compared to the $I4_1/a$ α phase, which translates to very low barriers for rotation of the AlH_4^- tetrahedra and could be indirectly related to the observation of the "S105" shift recently reported in NMR studies [7, 8, 17]. It is worth noting that the $Cmcm$ and $Fmm2$ phases are structurally difficult to distinguish upon thermal disordering of the low-frequency AlH_4^- rotational modes, suggesting the two phases should have very similar

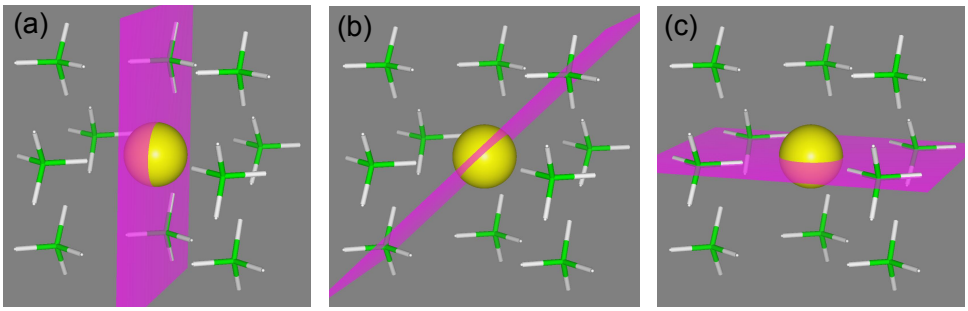

FIG. 1: The AlH_4^- vacancy (central yellow sphere) and its neighboring AlH_4^- tetrahedra. The highlighted planes in (a), (b), and (c) represent the (010), $(0\bar{1}1)$, and (001) lattice planes, respectively, in which an AlH_4^- neighbor can diffuse to the vacancy site.

finite-temperature diffusive properties.

In this Letter, we demonstrate by first-principles total-energy and molecular dynamics (MD) calculations that the diffusion barriers for AlH_3-related vacancies, which play a critical role in mediating the long range transport of Al and the release of hydrogen [19], are significantly lower in the γ phase than in the α phase. These findings provide the missing link in the mass transport and further confirm the relevance of the γ phase and related high-entropy polymorphs in the hydrogen-releasing decomposition of $NaAlH_4$.

Total-energy calculations based on density functional theory are performed using a plane-wave basis as implemented within the VASP package [20, 21]. For the exchange-correlation functional the generalized gradient approximation in the form proposed by Perdew *et al.* [22] is used. The total-energy converges to 10^{-5} eV per cell in each self-consistent loop, and the structural relaxation terminates when the force on each atom is smaller than 0.01 eV/Å. Car-Parrinello molecular dynamics calculations are performed using the Quantum-ESPRESSO package [23], with the Perdew-Burke-Ernzerhof [24] exchange-correlation functional. The electron-ion interaction is described by Vanderbilt ultrasoft pseudopotentials [25] in both total-energy and MD calculations. A cut-off energy of 600 eV is used for the plane-wave basis (400 eV for the dynamics simulations). For charged vacancies, jellium-like compensating charges are added to the background in order to keep the structure charge-neutral. Dynamics simulations are run for 15 ps at 350 K in the canonical NVT ensemble with a time step of 5 a.u. and an effective electronic mass of 400 a.u., with temperatures maintained using Nosé-Hoover chains [26].

The AlH_4^- vacancy in γ-$NaAlH_4$ does not significantly change the local geometry. Figure 1 shows the vacancy (represented by the yellow sphere at the center) and its neighboring AlH_4^- anions, all of which maintain nearly perfect tetrahedral coordination. The diffusion of the vacancy takes place when one of the three inequivalent AlH_4^- neighbors, located in the (010), $(0\bar{1}1)$, and (001) lattice planes as highlighted in Fig. 1 (a), (b), and (c), respectively, diffuses to the vacancy site. The diffusion of the AlH_4^- anion in the (010) plane [Fig. 1 (a)] has the lowest energy barrier of 0.072 eV, calculated by the nudged elastic band (NEB) method [27], as shown in Fig. 2 (a). Along the diffusion path, the AlH_4^- anion keeps the tetrehedron shape, and merely rotates about the central Al atom. Other possible diffusion paths located in $(01\bar{1})$ and (001) planes have much larger energy barriers of 0.35 eV and 1.50 eV, respectively, due to enhanced steric hindrance from nereby sodium atoms. In contrast, the diffusion barrier for the AlH_4^- vacancy in α-$NaAlH_4$ is over 0.4 eV [10, 11], much larger than the lowest barrier in γ-$NaAlH_4$.

The dehydrogenation reaction releases Al and H atoms in a 1:3 ratio. Upon removal of an AlH_3 unit from an AlH_4^- anion, the remaining H ion recombines with a neighboring AlH_4^- anion and forms a new ${AlH_5}^{2-}$ anion, which tends to adopt a triangular bipyramid structure. Depending on which AlH_4^- anion the remaining H ion joins, three different final configurations can be formed as shown in Fig. 3, where the vacancy-AlH_5^{2-} pair sits in the (010), $(0\bar{1}1)$, and (001) planes, for Configurations A, B, and C, respectively. Configuration A has the lowest energy, and Configurations B and C are 0.002 and 0.012 eV less stable, respectively.

The NEB method failed to give a clean path for the diffusion of the AlH_3 vacancy due to the complicated vacancy structure. Similar difficulties were also met in a previous study of the α-phase [10]. Fortunately, it is possible to apply an alternative strategy by manually sampling the "diffusion coordinates", that is, the coordinates with respect to which the potential energy has a negative curvature at the transition state. At each sampling point, only the diffusion coordinates are fixed, while all the other degrees of freedom are allowed to relax. In this way, an "uphill" landscape of the potential energy is created, from which the diffusion barrier can be estimated. While this method cannot give the exact minimal energy path for the diffusion as the more demanding NEB method [27], it gives a reliable estimation of the energy barrier provided that a reasonably fine mesh is used for the sampling. A similar method was applied in the study of the dissociative adsorption of H_2 molecules on an Al

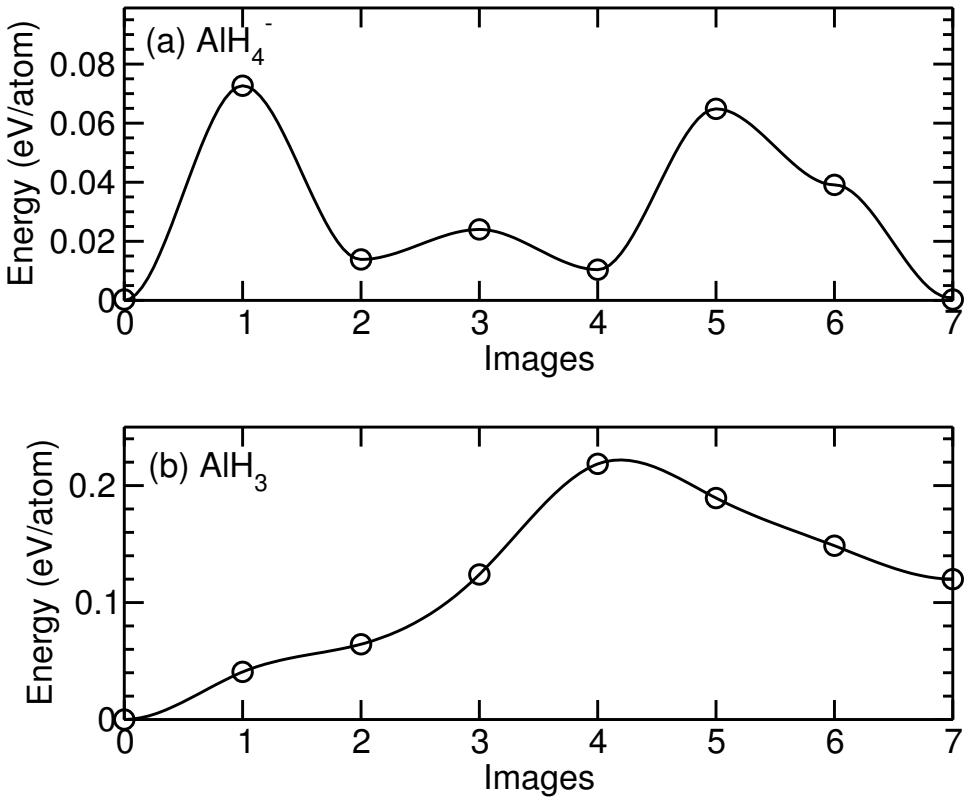

FIG. 2: (a) Energy landscape along the diffusion path for the AlH_4^- vacancy in γ-$NaAlH_4$, calculated by the NEB method. (b) Energy landscape along the diffusion path for the AlH_3 vacancy in γ-$NaAlH_4$, calculated by sampling the z-coordinate of the diffusing Al atom (the NEB method fails in this case).

surface [28].

An immediate diffusion route for the AlH_3 vacancy is that the entire AlH_5^{2-} anion moves toward the vacancy site. Only Configuration A in Fig. 3 was considered for this pathway, since the diffusion of the bulky AlH_5^{2-} complex in the other two configurations is expected to be largely blocked by nearby sodium atoms, as was the case for the diffusion of the AlH_4^- anion. But unlike the AlH_4^- anion, which keeps its shape during diffusion, the AlH_5^{2-} anion interacts with a nearby AlH_4^- anion located in the same (001) plane as the vacancy, and eventually loses the additional H atom to the latter. As a result, the diffusion process ends with Configuration C in Fig. 3. Figure 2 (b) shows the energy profile of this diffusion process sampled across the z coordinate of the central Al atom of the AlH_5^{2-} anion, which shows a diffusion barrier of about 0.22 eV. Nearly identical diffusion barriers were obtained when the x or $x - z$ values of the central Al atom were instead selected as the diffusion coordinate.

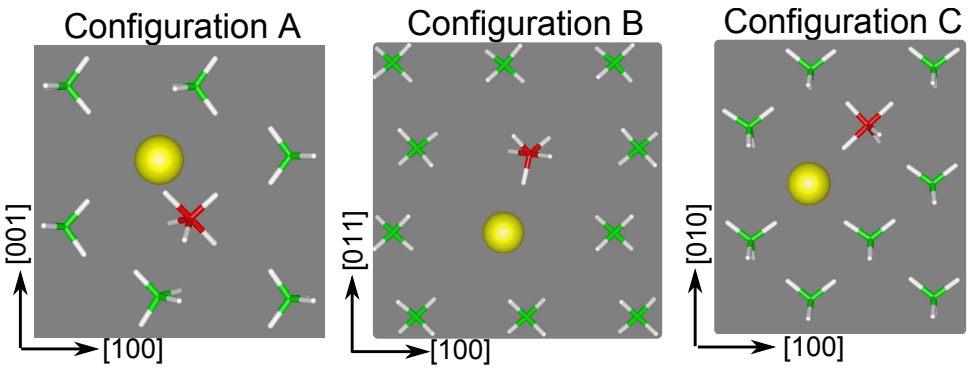

FIG. 3: Three different configurations for the AlH_3 vacancy in γ-$NaAlH_4$, in which the vacancy-AlH_5^{2-} pair sits in the (010) (Configuration A), $(0\bar{1}1)$ (Configuration B), and (001) (Configuration C) lattice planes. The central Al in AlH_5^{2-} is shown in red.

Again starting from Configuration A in Fig. 3, another possible diffusion pathway involves the AlH_5^{2-} anion separating into an AlH_4^- unit and an extra H. The former moves in the (010) plane toward the vacancy site, and the latter moves in the (001) plane and joins a nearby AlH_4^- anion. This process, outlined in Fig. 4 (a), transforms Configuration A into Configuration B. To evaluate its energy barrier, two diffusion coordinates were chosen, describing the movement of the AlH_4^- unit and the extra H ion, respectively. A contour plot shown in Fig. 4 (b) was created by sampling across these two diffusion coordinates, from which we derived a diffusion barrier of less than 0.1 eV. This energy barrier is close to the barrier for the diffusion of the AlH_4^- anion itself, indicating that the separation of the AlH_5^{2-} anion does not need to overcome a large energy barrier.

The calculated migration barriers are sufficiently low that they should be observable on the time-scales accessible to first-principles molecular dynamics (FPMD). Accordingly, we performed FPMD on 192-atom supercells of bulk γ-$NaAlH_4$ in the presence of AlH_4^- and AlH_3 vacancies. Starting configurations were the same as those used for the in our total-energy calculations, although the systems were first allowed to thermalize to 350 K. For comparison, a set of simulations was also performed on bulk α-$NaAlH_4$ with these same vacancies, with the cell volume constrained to prevent the $\alpha \rightarrow \gamma$ transition.

All three of the reported low-barrier diffusion mechanisms in γ-$NaAlH_4$ are directly observed in FPMD simulations. Figure 5 shows cooperative diffusion events of the AlH_4^- vacancy, following the mechanism of Fig. 2 (a). Diffusion in the presence of an AlH_3 vacancy is shown in Fig. 6, following the mechanisms of Fig. 2 (b) and the reverse process of

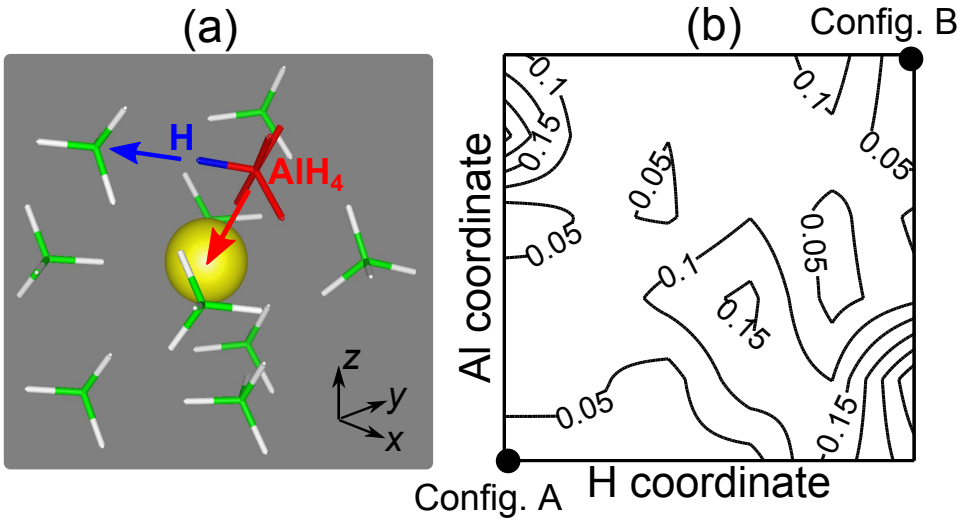

FIG. 4: (a) Schematic illustration of a possible diffusion path for the AlH_5^{2-} anion in γ-$NaAlH_4$, in which it separates into an AlH_4^- unit (red) and an extra H ion (blue). Red and blue arrows point to the destination for the AlH_4^- unit and the extra H ion, respectively. (b) Contour plot of the energy landscape by sampling the coordinates of the extra H atom and the central Al in the AlH_4^- unit. Configurations A and B, the beginning and final configurations, respectively, are labeled. Contour lines are in units of eV.

Fig. 4. Note that in every case, net vacancy diffusion is anisotropic and proceeds between successive (001) crystal planes.

For the AlH_3 vacancy (Fig. 6), the choice of diffusion mechanism is based on the location of the remaining hydrogen, which attaches to a nearby AlH_4^- tetrahedron to form AlH_5^{2-}. If the AlH_5^{2-} is in a different (001) crystal plane from the vacancy, then the mechanism of Fig. 6 (a–d) is used. If instead it is in the same plane, then the mechanism of Fig. 6 (e–h) becomes active. In both cases, the dynamics show that an intermediate $Al_2H_9^{3-}$ complex is formed when an axial hydrogen in the bipyramidal AlH_5^{2-} binds with the destination tetrahedron immediately prior to its transfer.

The dynamics simulations of γ-$NaAlH_4$ illustrate some subtle structural changes that are induced by the presence of vacancies. For instance, in each of the snapshots, there is a weak binding between the positively charged vacancy and one of its anion neighbors. This can be seen in the distortion of the anion center from its ideal lattice site towards the vacancy. On average, the magnitude of this distortion is on the order of 1.0–1.5 Å. The influence of the vacancy on the surrounding tetrahedra does not appear to be uniform,

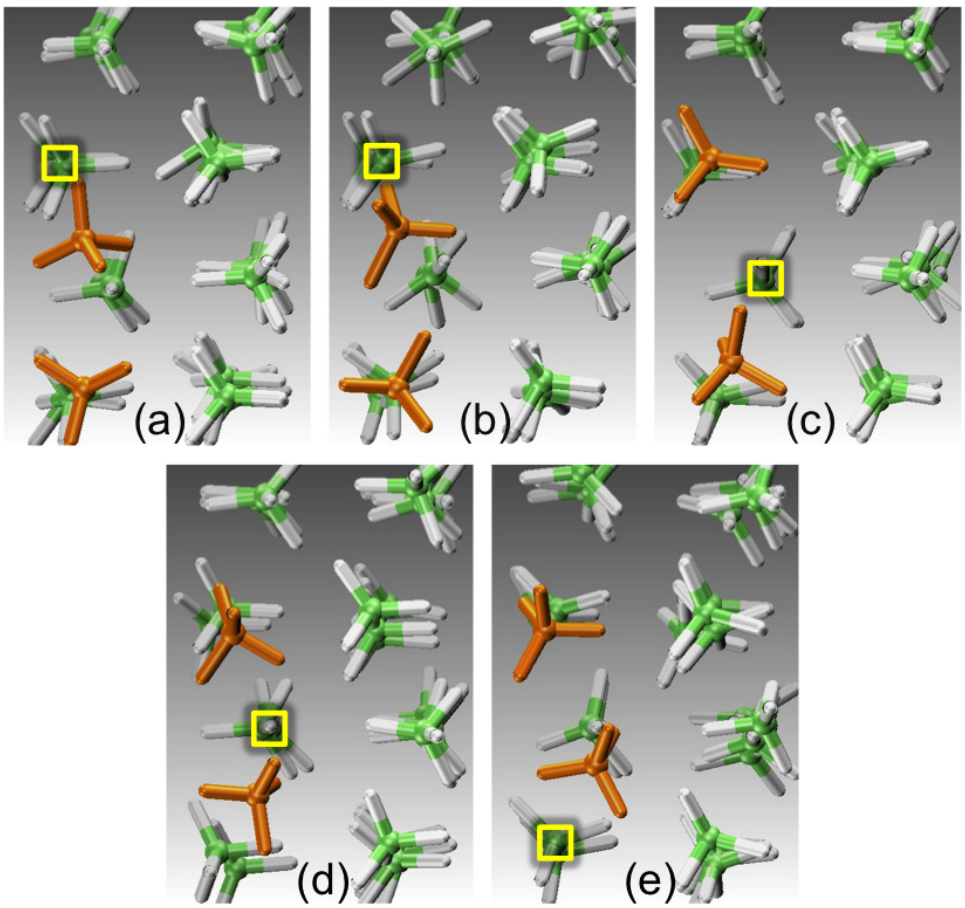

FIG. 5: Diffusion of an AlH_4^- vacancy in γ-$NaAlH_4$ via the mechanism of Fig. 2 (a), as taken from FPMD snapshots. The vacancy site is indicated by a yellow square, and the diffusing AlH_4^- tetrahedra are highlighted in orange. Two distinct diffusion events are observed, involving two different tetrahedra (a–c and d–e). Horizontal and vertical directions represent $[0\bar{1}0]$ and [001], respectively.

but instead preferentially forms a single vacancy-anion pair; this suggests the nature of the interaction is not exclusively electrostatic. Notably, this neighbor is the one that becomes involved in diffusion, probably because the reduced distance to the vacancy shortens the reaction pathway. The interaction between the vacancy and the anion is highlighted in the two diffusion events in Fig. 5. Upon completion of the first diffusion event, the diffusing tetrahedron settles into what is more or less the ideal lattice site, indicating the weak binding to the vacancy is broken. Instead, a new anion-vacancy pair is formed, and this new anion becomes the agent in the second diffusion event.

The tetrahedra in successive (001) crystal planes of both the α and γ phases have opposite

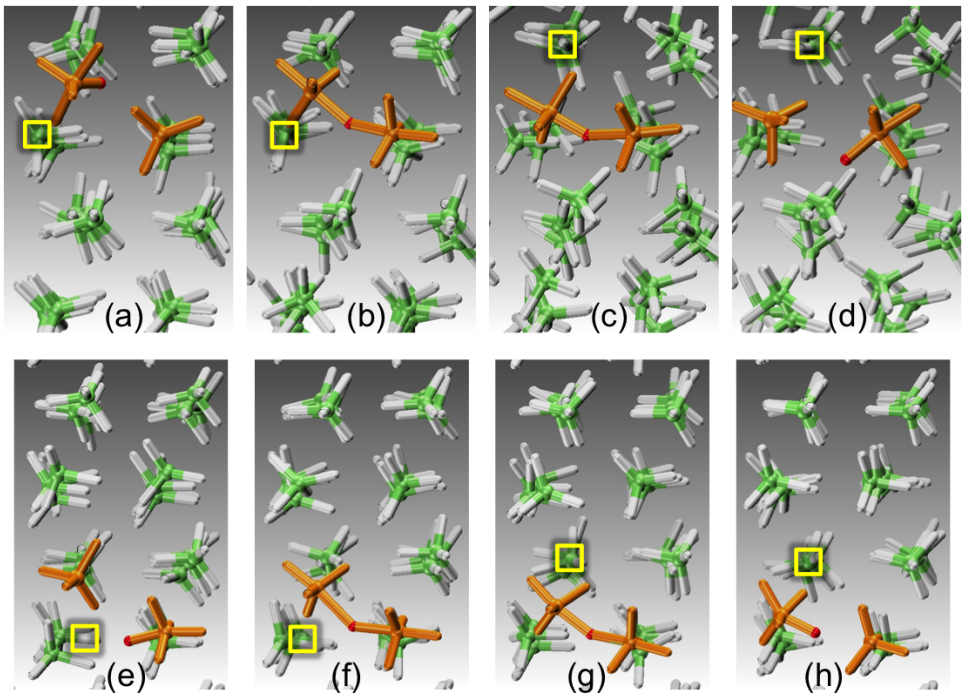

FIG. 6: Diffusion of an AlH_3 vacancy in γ-$NaAlH_4$, as taken from FPMD snapshots. The vacancy site is indicated by a yellow square. The involved AlH_4^- tetrahedra are highlighted in orange, and the diffusing hydrogen is shown in red. Horizontal and vertical directions represent $[0\bar{1}0]$ and [001], respectively. Panels (a–d) show the mechanism of Fig. 2 (b), for which the orphan hydride begins attached to an AlH_4^- tetrahedron in a different (001) plane from the vacancy site. Panels (e–h) show the reverse process of Fig. 4, for which the orphan hydride begins attached to an AlH_4^- tetrahedron in the same (001) plane as the vacancy site.

orientations. In principle, diffusion between these planes must therefore be accompanied by rotation of the tetrahedral complexes. This process is significantly easier in γ-$NaAlH_4$ because of its larger free volume. In fact, the elevated-temperature structure of γ-$NaAlH_4$ has more entropically driven native rotational disorder of the tetrahedra, which allows for a drastically lower reorientational barrier.

In contrast to the γ-$NaAlH_4$ results, dynamics simulations of α-$NaAlH_4$ did not reveal any AlH_x diffusion events within the 15 ps simulation time. This agrees with reports of a much higher diffusion barrier for all vacancy complexes [10, 11]. For the AlH3 vacancy simulation in α-$NaAlH_4$, we did observe dynamical exchanges of the orphan hydride between AlH_4^- tetrahedra, as reported by Gunaydin *et al.* [19] Similar to their findings, the hydride

exchanges were always confined to tetrahedra neighboring the vacancy site, evidencing the Coulomb interaction between the vacancy and AlH_5^{2-} complexes. However, no vacancy or Al diffusion was observed, inhibiting long-range diffusion on the time-scales accessible to the simulations.

To conclude, the diffusion barriers for AlH_4^- and AlH_3 vacancies in γ-$NaAlH_4$ were calculated to be lower than 0.1 eV by sampling the potential energy surface using first-principles methods. First-principles molecular dynamics simulations on picosecond time-scales directly observed all the predicted diffusion pathways, reconfirming their ultra-low energy barriers. Our results suggest that γ-$NaAlH_4$ (or one that shares its essential structural features) participates in the dehydrogenation process of α-$NaAlH_4$ as an intermediate phase, and ultimately accounts for the fast mass transport observed in experiments. Since the long-range diffusion is sufficiently fast, the actual rate-limiting process could be associated with the phase transition kinetics between the α phase and the intermediate γ phase. In this scenario, the overall reaction kinetics should improve if one can find ways to facilitate the $\alpha \rightarrow \gamma$ transition. One possibility is to reduce the domain size, since the γ phase has lower surface energy than the α phase [16]. Indeed, recent experiments observed enhancement in kinetic performance when $NaAlH_4$ is incorporated into a nanoporous matrix [13, 14]. Moreover, this interpretation suggests that the mysterious role that transition metal catalysts play in this system [29–31] could be linked to the nucleation of γ-like phases. Accordingly, a highly desirable follow-up study would be to investigate the effects of transition metals such as Ti on the thermodynamics and kinetics of the intermediate phase transitions.

This work is supported by the U.S. Department of Energy, Office of Basic Energy Sciences, Division of Materials Sciences and Engineering under Award DE-FG02-97ER45632. This research uses resources of the National Energy Research Scientific Computing Center (NERSC), which is supported by the Office of Science of the U.S. Department of Energy Under Contract No. DE-AC02-05CH11231. A portion of this work was performed under the auspices of the U.S. Department of Energy by Lawrence Livermore National Laboratory under Contract DE-AC52-07NA27344.

* Electronic address: meiyin.chou@physics.gatech.edu

[1] J. Tollefson, Nature **464**, 1262 (2010).

[2] B. Bogdanović and M. Schwickardi, J. Alloys Compd. **253**, 1 (1997).

[3] M. P. Pitt, P. E. Vullum, M. H. Sorby, H. Emerich, M. Paskevicius, C. E. Buckley, E. Mac, A. Gray, J. C. W. Salmsley, R. Holmestad, and B. C. Hauback, Phil. Mag. **93**, 1080 (2013).

[4] K. J. Gross, S. Guthrie, S. Takara, and G. Thomas, J. Alloys and Compd. **297**, 270 (2000).

[5] O. Palumbo, A. Paolone, R. Cantelli, C. M. Jensen, and R. Ayabe, Mat. Sci. Eng. A **442**, 75 (2006).

[6] R. Cantelli, O. Palumbo, A. Paolone, C. M. Jensen, M. T. Kuba, and R. Ayabe, J. Alloys Compd. **446–447**, 260 (2007).

[7] T. M. Ivancic, S.-J. Hwang, R. C. Bowman, Jr., D. S. Birkmire, C. M. Jensen, T. J. Udovic, and M. S. Conradi, J. Phys. Chem. Lett. **1**, 2412 (2010).

[8] E. G. Sorte, R. C. Bowman, Jr., E. H. Majzoub, M. H. W. Verkuijlen, T. J. Udovic, and M. S. Conradi, J. Phys. Chem. C **117**, 8105 (2013).

[9] A. Borgschulte, A. Züttel, P. Hug, G. Barkhordarian, N. Eigen, M. Dornheim, R. Bormann, and A. J. Ramirez-Cuesta, Phys. Chem. Chem. Phys. **10**, 4045 (2008).

[10] G. B. Wilson-Short, A. Janotti, K. Hoang, A. Peles, and C. G. Van de Walle, Phys. Rev. B **80**, 224102 (2009).

[11] K. J. Michel and V. Ozoliņš, J. Phys. Chem. C **115**, 21465 (2011).

[12] R. K. Bhakta, S. Maharrey, V. Stavila, A. Highley, T. Alam, E. Majzoub, and M. Allendorf, Phys. Chem. Chem. Phys. **14**, 8160 (2012).

[13] C. P. Baldé, B. P. C. Hereijgers, H. Bitter, and K. P. de Jong, Angew. Chem. Int. Ed. **45**, 3501 (2006); J. Am. Chem. Soc. **130**, 6761 (2008).

[14] R. D. Stephens, A. F. Gross, S. L. Van Atta, J. J. Vajo, and F. Pinkerton, Nanotechnology **20**, 204018 (2009).

[15] A. Zaluska, L. Zaluski, and J. O. Ström-Olsen, J. Alloys Compd. **298**, 125 (2000).

[16] B. Wood and N. Marzari, Phys. Rev. Lett. **103**, 185901 (2009); **104**, 019901 (2009).

[17] E. H. Majzoub, E. Hazrati, and G. A. de Wijs, J. Phys. Chem. C **117**, 8864 (2013).

[18] H. Yukawa, N. Morisaku, Y. Li, K. Komiya, R. Rong, Y. Shinzato, R. Sekine, and M. Moringaga, J. Alloys Compd. **446-447**, 242 (2007).

[19] Gunaydin H., Houk K.N. & Ozoliņš V. Proc. Natl. Acad. Sci. USA **105**, 3673-3677 (2008).

[20] G. Kresse and J. Furthmüller, Phys. Rev. B **54**, 11169 (1996).

[21] G. Kresse and J. Furthmüller, Comput. Mater. Sci. **6**, 15 (1996).

[22] J. P. Perdew, J. A. Chevary, S. H. Vosko, K. A. Jackson, M. R. Pederson, D. J. Singh, and C. Fiolhais, Phys. Rev. B **46**, 6671 (1992).

[23] P. Giannozzi *et al.*, J. Phys. Condens. Matt. **21**, 395502 (2009).

[24] J. P. Perdew, K. Burke, and M. Ernzerhof, Phys. Rev. Lett. **77**, 3865 (1996).

[25] D. Vanderbilt, Phys. Rev. B **41**, 7892 (1990).

[26] G. J. Martyna and M. L. Klein and M. E. Tuckerman, J. Chem. Phys. **97**, 2635 (1992).

[27] G. Henkelman and H. Jónsson, J. Chem. Phys. **113**, 9978 (2000).

[28] B. Hammer, K. W. Jacobsen, and J. K. Nørskov, Phys. Rev. Lett. 69, 1971 (1992).

[29] S. I. Orimo, Y. Nakamori, J. R. Eliseo, A. Zuttel, and C. M. Jensen, Chem. Rev. **107** 4111 (2007).

[30] B. Sakintuna, F. Lamari-Darkrim, and M. Hirscher, Int. J. Hygrogen Energ. **32**, 1121 (2007).

[31] T. J. Frankcombe, Chem. Rev. **112 (4)**, 2164 (2012).